A multiscale analytical approach for bone remodeling simulations : linking scales from collagen to trabeculae

Bone 64 (2014) 303–313

Contents lists available at ScienceDirect

Bone

journal homepage: www.elsevier.com/locate/bone

A multiscale analytical approach for bone remodeling simulations: Linking scales from collagen to trabeculae

Michele Colloca [a], Romane Blanchard [b], Christian Hellmich [b], Keita Ito [a], Bert van Rietbergen [a,*]

[a] Orthopaedic Biomechanics, Department of Biomedical Engineering, Eindhoven University of Technology, The Netherlands
[b] Institute for Mechanics of Materials and Structures, Vienna University of Technology, Austria

ARTICLE INFO

Article history:
Received 23 August 2013
Revised 24 March 2014
Accepted 25 March 2014
Available online 5 April 2014

Edited by: David Fyhrie

Keywords:
Multiscale
Bone remodeling
Bone volume fraction
Collagen
Analytical modeling

ABSTRACT

Bone is a dynamic and hierarchical porous material whose spatial and temporal mechanical properties can vary considerably due to differences in its microstructure and due to remodeling. Hence, a multiscale analytical approach, which combines bone structural information at multiple scales to the remodeling cellular activities, could form an efficient, accurate and beneficial framework for the prognosis of changes in bone properties due to, e.g., bone diseases. In this study, an analytical formulation of bone remodeling integrated with multiscale micromechanical models is proposed to investigate the effects of structural changes at the nanometer level (collagen scale) on those at higher levels (tissue scale). Specific goals of this study are to derive a mechanical stimulus sensed by the osteocytes using a multiscale framework, to test the accuracy of the multiscale model for the prediction of bone density, and to demonstrate its multiscale capabilities by predicting changes in bone density due to changes occurring at the molecular level.

At each different level, the bone composition was modeled as a two-phase material which made it possible to: 1) find a closed-form solution for the energy-based mechanical stimulus sensed by the osteocytes and 2) describe the anisotropic elastic properties at higher levels as a function of the stiffness of the elementary components (collagen, hydroxyapatite and water) at lower levels. The accuracy of the proposed multiscale model of bone remodeling was tested first by comparing the analytical bone volume fraction predictions to those obtained from the corresponding μFE-based computational model. Differences between analytical and numerical predictions were less than 1% while the computational time was drastically reduced, namely by a factor of 1 million. In a further analysis, the effects of changes in collagen and hydroxyapatite volume fractions on the bone remodeling process were simulated, and it was found that such changes considerably affect the bone density at the millimeter scale. In fact, smaller tissue density induces remodeling activities leading to finally higher overall bone density. The multiscale analytical model proposed in this study potentially provides an accurate and efficient tool for simulating patient-specific bone remodeling, which might be of importance in particular for the hip and spine, where an accurate assessment of bone micro-architecture is not possible.

Introduction

Bone is a dynamic porous material which is continuously resorbed and subsequently formed in a process called bone remodeling influenced by both mechanical and biological factors [1–5]. Moreover, it is a hierarchical material whose architecture differs at each level of hierarchy and whose mechanical properties can vary considerably, even on the same specimen, due to bone heterogeneity [6–8]. The density of bone is modulated by two groups of cells: the osteoclasts which resorb bone and osteoblasts which deposit new bone [9]. The actions of these actor cells are thought to be mediated by osteocytes which are the most numerous cells in the bone. It has been hypothesized that the osteocytes can sense the local mechanical stimulus, in turn controlling the activity of osteoblasts and osteoclasts within a basic multicellular unit (BMU) [10–12].

Several mathematical models have been proposed in an attempt to elucidate the features of bone adaptation at the different scales, though at the organ, tissue and cell level, these models merely exist in isolation [13]. By integrating numerical equations into finite element models, it was shown that the load-driven bone remodeling algorithm based on mechanosensory theory can explain many features of bone adaptation at the tissue- and cell-level [14,15], e.g. the formation of load-adapted microstructures, as well as the loss of bone mass and microstructural integrity after disuse or increased osteoclast activity (associated with decreased estrogen levels). However, using such analyses for patient-

* Corresponding author.
E-mail address: b.v.rietbergen@tue.nl (B. van Rietbergen).

http://dx.doi.org/10.1016/j.bone.2014.03.050
8756-3282/

specific predictions of bone remodeling is difficult because of the limited resolution of in-vivo imaging techniques and the huge computational cost involved for such detailed bone remodeling analyses.

A method to reduce the computational time in the abovementioned analyses and to deal with the fact that at most sites (e.g. hip and spine) no patient bone microarchitecture can be measured would be to implement the bone remodeling theory in a multi-scale framework that can translate structural changes at the cell-level to changes in bone density at the organ level. By using an analytical formulation of the bone remodeling equation integrated with multiscale micromechanical models, that use generalized structural models at each level of organization [16], such multi-step homogenization schemes can provide a very flexible framework to derive mechanical properties at any level. By integrating such models with bone remodeling equations, it will be possible to predict bone remodeling at these different levels in a very efficient manner.

The concept of integrating multi-scale modeling and bone remodeling has been introduced in earlier studies. Coelho et al. [17] presented a multiscale model for bone tissue adaptation that considered two levels, whole bone and trabecular architecture. The bone density distribution predictions were evaluated at the macroscale level, taking into account mechanical properties as well as surface density and permeability of the trabecular structure at the microscale level. Hambli et al. [18] developed a multiscale approach for bone remodeling simulation integrating finite element models at the macro level and 3D neural network computation techniques at the mesolevel. The authors did not, however, include in their bone remodeling formulation cellular activities and biological factors that affect bone apposition and resorption. In their investigation, Podshivalov et al. [19] presented a new 3D multiscale FE method based on domain-based multiresolution hierarchical geometric modeling and multiscale material properties of trabecular bone. The goal was to design a computational tool as infrastructure for computerized systems aiming at interactively analyzing bone structures. None of these models can explicitly account at the nanolevel for collagen and hydroxyapatite contributions on stiffness and volume fraction of the bone tissue at higher levels. Also, most of these studies rely on computational tools to solve equations at each included level, whereas a true multiscale approach would benefit from an analytical description that spans multiple levels.

Going in the direction to integrate bone structural information at different scales and the remodeling process, in recent works [20,21] we proposed an analytical model in which the bone remodeling process was studied on the basis of two connected scales, tissue and cell levels respectively, with the dependency on osteoblast and osteoclast activities in terms of bone apposition and resorption rates and on the estimation of strain energy density (SED), as mechanical stimulus. In that work, we were able to show that organ-level bone remodeling models that represented the bone microstructure by a simplified regular structure could predict bone density changes in good agreement with micro-structural models that represented the actual micro-architecture. However, the results were limited to two levels only and the remodeling signal was based on the average tissue-level SED, whereas for the bone remodeling more accurate SED values at the bone matrix surfaces are necessary.

In the present study we therefore extend this work by combining the earlier developed remodeling theory with a multi-scale framework that can account for (changes in) bone mechanical properties at all levels of bone structural organization (Fig. 1). Using this model it is possible to get more accurate estimates of the stresses that the osteocytes sense by using more elaborate models of the bone microstructure and bone tissue composition. In particular, specific goals of this study are: 1) to derive, as mechanical stimulus sensed by the osteocytes, the micromechanics-derived SED based on an Eshelby matrix-inclusion problem in order to accurately and efficiently predict the stress distributions in a representative volume element of trabecular bone; 2) to test the accuracy of the multiscale analytical model by comparing the bone volume fraction predictions to those obtained from the earlier computational models that represent the full bone microstructure; and 3) to demonstrate its multiscale capabilities by investigating in children bones the effects of age-dependent changes in collagen and hydroxyapatite content that are defined at the nanometer scale, on the bone volume fraction at the millimeter scale.

Methods

Analytical approach for bone remodeling simulations

In the bone remodeling theory adopted for this study, it is assumed that the osteocytes inside the bone tissue sense mechanical loading and transmit a signal to the osteoblasts on the bone matrix surface to form bone, while the osteoclasts are assumed to be attracted by effects of local micro-damage [22]. The formulation of this theory as implemented in a validated analytical model [21] is expressed in terms of net linear rate $dl_{BM}(x,t)/dt$ of bone apposition or resorption of bone matrix at a particular trabecular surface location x at time t determined by

$$\frac{dl_{BM}}{dt} = \frac{dl_{OBL}(x,t)}{dt} - \frac{dl_{OCL}(x,t)}{dt} \tag{1}$$

where $dl_{OBL}(x,t)/dt$ and $dl_{OCL}(x,t)/dt$ are the linear bone formation rate ($\mu m/day$) and linear bone resorption rate ($\mu m/day$), respectively.

Bone remodeling is assumed to occur on the internal surfaces of the bone matrix or on the walls of the voids and the rate of change of bone volume fraction is influenced by the amount of internal surface available for cellular activity as experimentally evidenced [9,10].

In the multiscale analytical framework proposed in this study, remodeling equations at the tissue level, that can account for bone tissue properties as determined by lower levels (cell and collagen levels) and that can represent the bone density evolution at higher levels (e.g. organ level), are developed (Fig. 1). As a starting point, we consider the analytical expression of the rate of change of bone volume fraction in the RVE of trabecular bone at the tissue level, when modulated by mechanobiological and geometric feedback as given in [23],

$$\frac{d(BV/TV)}{dt} = \left(\frac{dl_{OBL}(x,t)}{dt} - \frac{dl_{OCL}(x,t)}{dt}\right) \cdot \alpha \cdot BS/TV \tag{2}$$

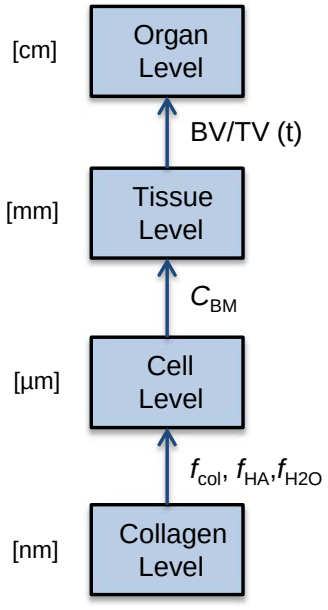

Fig. 1. Block-diagram of the proposed multiscale analytical model. Volume fraction of hydroxyapatite (f_{HA}), collagen (f_{col}) and water (f_{H2O}) at the nano scale affect the stiffness of the bone matrix (C_{BM}) at the micrometer scale, which in turn affect the strain energy density and bone volume fraction change over time (t) at the millimeter scale.

with α as a fraction of the bone specific surface BS/TV ($\mu m^2/\mu m^3$) that is available for the cellular activities and expressed as a function of the bone volume fraction (BV/TV) by adopting the relationship of Martin [24]:

$$\frac{BS}{TV} = 0.0323 \cdot \left(1-\frac{BV}{TV}\right) - 0.0939 \cdot \left(1-\frac{BV}{TV}\right)^2 + 0.134 \cdot \left(1-\frac{BV}{TV}\right)^3 - 0.101 \cdot \left(1-\frac{BV}{TV}\right)^4 + 0.0288 \cdot \left(1-\frac{BV}{TV}\right)^5. \quad (3)$$

For the bone apposition activity through osteoblasts (dL_{OBL}/dt), we adopt the following expression

$$\frac{dl_{OBL}}{dt} = \tau \cdot \mu \cdot \psi_{BM} \quad (4)$$

where τ is the bone formation time constant ($\mu m^3/(nmol \cdot day)$), μ the osteocyte mechanosensitivity ($nmol/(MPa \cdot \mu m^2)$) and ψ_{BM} (MPa) is the "microscopic" strain energy density as "felt" by the osteocytes being uniformly dispersed into the bone matrix. It is derived from a continuum micromechanics model based on Eshelby's matrix-inclusion problem, as described in the following section in more detail.

For the bone resorption activity through osteoclasts, we adopt the following relationship

$$\frac{dl_{OCL}(x,t)}{dt} = A_{ocl} \quad (5)$$

with a constant resorption rate A_{ocl} ($\mu m/day$).

Eq. (2) represents a nonlinear differential equation of the first order that, in addition to the initial condition $\frac{BV}{TV}(t=0)$, forms an initial value problem to be solved numerically.

Micromechanics-derived strain energy density as mechanobiological stimulus

The microscopic strain energy density in the trabecular bone RVE (Fig. 2) is assumed as the mechanical stimulus sensed by the osteocytes regulating the bone remodeling process. It is defined by means of an Eshelby-problem micromechanics model [25], similar to that having undergone extensive experimental validation in Ref. [7] and to that used for micromechanics-supported finite element models of human mandibles to simulate the effects of atrophy on the bone density distribution [26].

Moreover, it is assumed that the macroscopic stress states act on the boundary of a trabecular bone RVE with their magnitudes equivalent to the maximum strain energy density rate [14], and that the direction of principal stresses e_I, e_{II}, e_{III} (with stress tensors $\Sigma = \Sigma_{11} e_I \otimes e_I + \Sigma_{22} e_{II} \otimes e_{II} + \Sigma_{33} e_{III} \otimes e_{III}$) coincide with the material directions of the transversely isotropic material. For this specific case, the "microscopic" strain energy density at the level of the solid bone matrix reads as

$$\psi_{BM} = \frac{1}{2} \boldsymbol{\varepsilon}_{BM} : \mathbb{C}_{BM} : \boldsymbol{\varepsilon}_{BM} \quad (6)$$

where $\boldsymbol{\varepsilon}_{BM}$ is the average (microscopic) strain tensor in the solid bone matrix, which is related to the macroscopic strain tensor (E) through the fourth-order concentration tensors $\mathbb{A}_{BM}$

$$\boldsymbol{\varepsilon}_{BM} = \mathbb{A}_{BM} : \boldsymbol{E} \quad (7)$$

where

$$\mathbb{A}_{BM} = \left\{ \varphi \left[\mathbb{I} + \mathbb{P}_{cyl}^{BM} : (\mathbb{C}_P - \mathbb{C}_{BM}) \right]^{-1} + (1-\varphi)\mathbb{I} \right\}^{-1} \quad (8)$$

being a function of the porosity φ, the stiffness tensor of the bone matrix $\mathbb{C}_{BM}$, the stiffness tensor of the porosity $\mathbb{C}_P$ and of Hill's morphology tensor expressed by

$$\mathbb{P}_{cyl}^{BM} = \begin{pmatrix} P_{1111}^{BM} = P_{2222}^{BM} & P_{1122}^{BM} & P_{1133}^{BM} = 0 \\ P_{2211}^{BM} = P_{1122}^{BM} & P_{2222}^{BM} = P_{1111}^{BM} & P_{2233}^{BM} = 0 \\ 0 & 0 & 0 \end{pmatrix}_{e_I,\ e_{II},\ e_{III}} \quad (9)$$

with the components of $\mathbb{P}_{ijkl}^{BM}$ according to Eq. (76) to (81) of Ref. [27]:

$$P_{1111}^{BM} = P_{2222}^{BM} = \frac{1}{8} \frac{(5C_{1111} - 3C_{1122})}{(C_{1111} - C_{1122})C_{1111}} \quad (10)$$

$$P_{1122}^{BM} = -\frac{1}{8} \frac{(C_{1111} + C_{1122})}{(C_{1111} - C_{1122})C_{1111}} \quad (11)$$

$$P_{2323}^{BM} = P_{1313}^{BM} = \frac{1}{8\, C_{2323}} \quad (12)$$

$$P_{1212}^{BM} = \frac{1}{8} \frac{(3C_{1111} - C_{1122})}{(C_{1111} - C_{1122})C_{1111}}. \quad (13)$$

Choosing the base frame to coincide with the aforementioned material directions, the stiffness of the bone matrix reads as

$$\mathbb{C}_{BM} = \begin{pmatrix} C_{1111} & C_{1122} & C_{1133} \\ C_{1122} & C_{1111} & C_{1133} \\ C_{1133} & C_{1133} & C_{3333} \end{pmatrix}_{e_I,\ e_{II},\ e_{III}}. \quad (14)$$

In fact, the bone matrix is characterized by a transversely isotropic elasticity tensor and modeled as mineral foam of hydroxyapatite which is "reinforced" predominantly in the longitudinal direction by collagen fibrils, while the transverse stiffness is mainly governed by the mineral concentration. Relevant values for this tensor will be introduced in the section entitled Micromechanics-derived bone matrix stiffness in adults and children.

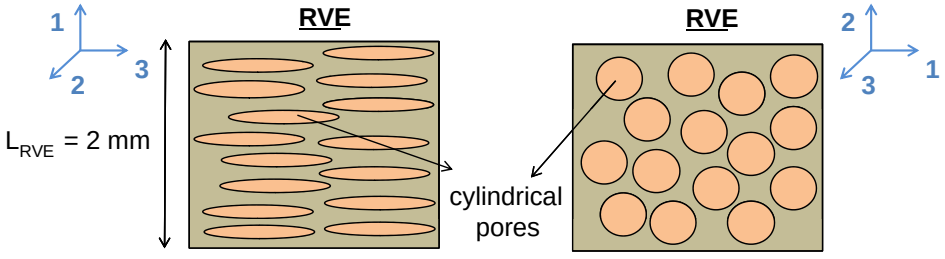

Fig. 2. Trabecular bone RVE modeled as a two-phase material: bone matrix and cylindrical inclusions. In the base frame, 1 is the radial direction, 2 the circumferential direction, and 3 the axial direction.

The stiffness tensor of the porosity $\mathbb{C}_P$ was chosen as that of fat $\mathbb{C}_{\mathrm{Fat}}$ and expressed in function only of the bulk modulus k_{Fat} by using the corresponding elastic constants given in [28]

$$\mathbb{C}_{\mathrm{Fat}} = 3k_{\mathrm{Fat}}\mathbb{J} \tag{15}$$

with $\mathbb{J}$ the volumetric part of fourth-order identity tensor $\mathbb{I}$ where

$$\mathbb{J}_{ijkl} = \frac{1}{3}\delta_{ij}\delta_{kl} \quad with \quad \begin{cases} \delta_{ij} = 1 & if \quad i = j \\ \delta_{ij} = 0 & otherwise \end{cases} \tag{16}$$

Hence

$$\mathbb{C}_{\mathrm{Fat}} = 3k_{\mathrm{Fat}}\mathbb{J} = 3k_{\mathrm{Fat}}\begin{pmatrix} 1/3 & 1/3 & 1/3 \\ 1/3 & 1/3 & 1/3 \\ 1/3 & 1/3 & 1/3 \end{pmatrix} = \begin{pmatrix} k_{\mathrm{Fat}} & k_{\mathrm{Fat}} & k_{\mathrm{Fat}} \\ k_{\mathrm{Fat}} & k_{\mathrm{Fat}} & k_{\mathrm{Fat}} \\ k_{\mathrm{Fat}} & k_{\mathrm{Fat}} & k_{\mathrm{Fat}} \end{pmatrix} \tag{17}$$

Collecting all the terms entering Eq. (6), a closed-form expression for the microscopic strain energy density can be found:

$$\begin{aligned} \psi_{BM} = \frac{1}{2}\Big[& \left(A_{1111}{}^2 + A_{1122}{}^2\right)\left(2C^{BM}_{1122}E_{11}E_{22} + C^{BM}_{1111}\left(E_{11}{}^2 + E_{22}{}^2\right)\right) \\ & + 2A_{1122}\left(A_{1133}\left(C^{BM}_{1111} + C^{BM}_{1122}\right) + C^{BM}_{1133}\right)(E_{11} + E_{22})E_{33} \\ & + \left(2A_{1133}{}^2\left(C^{BM}_{1111} + C^{BM}_{1122}\right) + 4A_{1133}C^{BM}_{1133} + C^{BM}_{3333}\right)E_{33}{}^2 \\ & + 2A_{1111}\left(A_{1122}\left(2C^{BM}_{1111}E_{11}E_{22} + C^{BM}_{1122}\left(E_{11}{}^2 + E_{22}{}^2\right)\right)\right. \\ & \left. + A_{1133}\left(C^{BM}_{1111} + C^{BM}_{1122}\right)C^{BM}_{1133}\right)(E_{11} + E_{22})E_{33}\Big] \end{aligned} \tag{18}$$

and it is a function of φ, C^{BM}_{1111}, C^{BM}_{1122}, C^{BM}_{1133}, C^{BM}_{3333} and k_{Fat}. The components of the concentration tensor $\mathbb{A}_{BM}$ can be found in the Appendix A.

Micromechanics-derived bone matrix stiffness in adults and children

The stiffness of the bone matrix is time- and space-invariant in adult healthy tissue [26,29,30] and depends on its composition, i.e. on the volume fractions of its principal constituents, namely hydroxyapatite (HA), collagen (col), and water (H_2O). In [31], the average tissue elasticity properties were successfully identified through a coupled approach comprising 10 MHz pulse transmission ultrasound with universal rules governing the composition and the hierarchical mechanical functioning of mineralized tissues, resulting in the following stiffness tensor of extracellular bone tissue:

$$\begin{aligned} \mathbb{C}^{adult}_{BM} &= \begin{pmatrix} C_{1111} & C_{1122} & C_{1133} & 0 & 0 & 0 \\ C_{1122} & C_{1111} & C_{1133} & 0 & 0 & 0 \\ C_{1133} & C_{1133} & C_{3333} & 0 & 0 & 0 \\ 0 & 0 & 0 & 2C_{2323} & 0 & 0 \\ 0 & 0 & 0 & 0 & 2C_{2323} & 0 \\ 0 & 0 & 0 & 0 & 0 & 2C_{1212} \end{pmatrix} \\ &= \begin{pmatrix} 12.7 & 6.2 & 6.4 & 0 & 0 & 0 \\ 6.2 & 12.7 & 6.4 & 0 & 0 & 0 \\ 6.4 & 6.4 & 20.2 & 0 & 0 & 0 \\ 0 & 0 & 0 & 7.9 & 0 & 0 \\ 0 & 0 & 0 & 0 & 7.9 & 0 \\ 0 & 0 & 0 & 0 & 0 & 6.5 \end{pmatrix} \text{ in [GPa].} \end{aligned} \tag{19}$$

Although this composition is rather constant in healthy adults, it is known to vary during development and with diseases, e.g. osteogenesis imperfecta. This variation stems from a variation in the bone tissue composition, i.e. from its mineral, collagen, and water contents. The latter were derived from age-dependent weight fractions of ash per mass of dry bone WF^{dry}_{ash}, as provided by Currey [32], through the following steps: First, the ash fraction was converted into a mineral fraction [33],

$$WF^{dry}_{HA} = WF^{dry}_{ash} \times 1.066 \tag{20}$$

considering 6.6% of the bone mineral burning at ashing temperatures well beyond 600 °C [34], as encountered with a Bunsen burner as used by Currey [32]. This quantity is related to the apparent mineral mass density ρ^*_{HA} in physiological tissue, being proportional to the mineral concentration, through

$$\rho^*_{HA} = WF^{dry}_{HA}\left(\rho^{BM} - \rho^*_{H_2O}\right) \tag{21}$$

where ρ^{BM} is the mass density of the extracellular bone matrix, and $\rho^*_{H_2O}$ is the apparent mass density of water, i.e. the mass of water per volume of extracellular bone tissue. The extracellular mass density and the apparent mass densities of mineral (ρ^*_{HA}), of water $\left(\rho^*_{H_2O}\right)$, and of organics $\rho^*_{org} = \rho^{BM} - \rho^*_{HA} - \rho^*_{H_2O}$, are all related by bilinear functions, see Fig. 3(a), so that Eq. (21) allows for assigning to each of Currey's experimental values for WF^{dry}_{HA}, values for ρ^{BM}, ρ^*_{HA}, $\rho^*_{H_2O}$, and ρ^*_{org}, see Table 1. We observe that the tissue mass densities nicely approach the "adult" value of $\rho^{BM} = 1.90$ g/cm^3 identified in [31]. The aforementioned apparent mass density values give access to the volume fractions of hydroxyapatite, of collagen, and of water, via:

$$f_{HA} = \frac{\rho^*_{HA}}{\rho_{HA}}, \quad f_{col} = 0.9 \times \frac{\rho^*_{org}}{\rho_{org}}, \quad f_{H_2O} = \frac{\rho^*_{H_2O}}{\rho_{H_2O}} \tag{22}$$

with the real mass densities of water, organics and hydroxyapatite amounting to $\rho_{H_2O} = 1$ g/cm^3, $\rho_{org} = 1.41$ g/cm^3 [35], and $\rho_{HA} = 3$ g/cm^3 [35–37]. From the volume fractions of (22), we retrieve the age-dependent tissue mass density ρ^{BM} according to $\rho^{BM} = f_{HA}\rho_{HA} + f_{org}\rho_{org} + f_{H_2O}\rho_{H_2O}$, which we approximate by means of a linear fit between age and mass density ρ^{BM} (coefficient of determination $R^2 = 0.72$). Then, the general compositional rules given in [33] give access to tissue mineral and collagen content at any age, see Table 2 for chosen ages between 6 and 13 years. The corresponding age-dependent volume fractions of mineral, water, and collagen components served as inputs for the 4-step micromechanical homogenization scheme developed in [33], from which the stiffness tensors for the extracellular bone matrix were obtained, see Fig. 3(b) and Table 3. The stiffness increase with age as predicted in Table 3 agrees well with that observed in in-vivo ultrasound experiments on the *os calcis* bones of children aged 6 through 13 years [38].

Three-dimensional micro-FE and analytical test models for bone modeling and remodeling simulations

The test model represented a 2 × 2 × 2 mm bone cubic region consisting of 226,981 cubic voxels. Each voxel was considered as a hexahedral element containing eight integration points. An element-by-element FE solver was used to calculate the strain energy density in each cubic voxel by which the domain of interest was discretized [39]. The bone sample was loaded by tensile loading distributions in the orthogonal *x*, *y* and *z* directions, as displayed in Fig. 4. The applied loading magnitudes were chosen by means of a numerical model developed to estimate in vivo bone loading based on bone morphology [40]. In the analytical model the same stresses were assumed to work on the sides of the RVE, and the corresponding (micro-)stresses and (micro-)strains at the bone tissue level were determined to obtain the tissue level SED. Using the earlier developed computational bone remodeling simulation model that implements the micro-FE model, the development and adaptation of bone micro-architecture were simulated and, at each time point, the volume fraction was calculated and compared to the volume fraction predicted by the analytical model. In particular, in order to study the evolution of bone volume fraction by solving both the analytical and micro-FE initial value problems with their own initial conditions, two simulation series were performed. In the first one, the bone modeling simulation was obtained by starting from a regular grid (Fig. 4) as initial configuration. In the second one, starting with

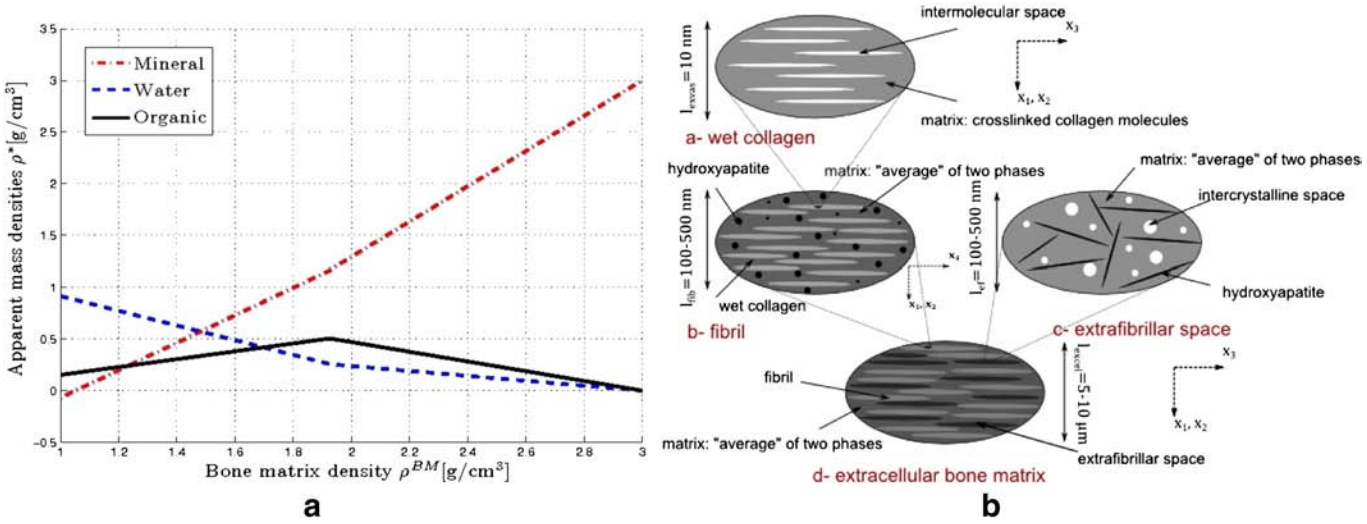

Fig. 3. a) Apparent mass densities of water, hydroxyapatite, and organic matter, as functions of the overall mass density of extracellular bone matrix, according to [33]; b) four-step homogenization scheme after [33].

the equilibrium condition reached in the first simulation series, changes in bone cellular activity, mechanotransduction and loading parameters were set to study their effects on the remodeling system response.

Results

In the following, we will use the term "analytical solution" when referring to the analytical model (Eq. (2)) and to the "numerical solution", which is taken as the reference, when referring to the bone remodeling algorithm that implements the micro-FE model, see section entitled Three-dimensional micro-FE and analytical test models for bone remodeling and remodeling simulations. In all cases, the % difference relative to the numerical predictions of bone volume fraction evolution was evaluated at equilibrium.

Bone modeling

The evolution of the RVE bone volume fraction is displayed in Fig. 5a where the numerical and analytical solutions are compared. Model parameters adopted in this simulation were defined according to bone physiological values as listed in Table 4. A regular grid (Fig. 5b) represented the initial configuration. After a transient period, the system reached an equilibrium condition in which the amount of bone formation was balanced by the amount of bone resorption; hence the bone volume fraction became constant. Initially BV/TV increased quickly as an effect of high mechanical signals, while resorption of poorly loaded tissue lagged behind as in Ref. [14]. Good agreement between analytical and numerical curves was found, with a difference less than 4% at the equilibrium, even though the transient behavior was different. In Fig. 5c, the final developed and adapted bone microstructure at equilibrium is shown.

Bone remodeling

Starting from the homeostatic bone microstructure of Fig. 5c, a second simulation was performed in which the osteoclast activity (A_{ocl}) was increased and the osteoblast activity (τ) was decreased by a factor of 10 with respect to the initial value. Such changes could, e.g. represent the effect of estrogen deficiency as in post-menopausal osteoporosis [41] in the first case, and the result of bone degenerative diseases [42] in the second one. In Fig. 6 the analytical and numerical outcomes with their corresponding adapted microstructures are compared, showing the expected bone loss in case of increased osteoclast activity (Figs. 6a–b) with a difference of 14.4% between predictions of the analytical and numerical models, and in case of decreased osteoblast activity (Figs. 6c–d) with a difference of 1%. During the transient phase, the analytical solution somewhat underestimated the bone density in case of τ decreasing.

A new simulation series was designed to predict changes in bone volume fraction after increasing the loading magnitude and the osteocyte mechanosensitivity (μ) to 200%, or decreasing them to 50% of the original value, respectively (Figs. 7–8). The numerical model showed the expected increase in bone mass with increased mechanosensitivity and loading magnitude, and the decrease after the reduction of the same parameters. The analytical models predicted these changes quantified in 13.3% difference for the increased loading case (Figs. 7a–b) and in 0.6% for the decreased loading case (Figs. 7c–d).

Table 1
Constituent volume fractions in juvenile femoral bone tissue tested by Currey [32] (HA = hydroxyapatite, col = collagen, H_2O = water).

Age (year) [32]	WF_{ash}^{dry} given [32]	WF_{HA}^{dry} Eq. (20)	ρ^{BM} Eq. (21)	ρ_{col}^{*} Fig. 3	ρ_{HA}^{*} Fig. 3	$\rho_{H_2O}^{*}$ Fig. 3
4.1	0.605	0.645	1.541	0.359	0.652	0.531
5.9	0.617	0.658	1.606	0.384	0.738	0.484
9.7	0.640	0.682	1.773	0.447	0.960	0.366
11.8	0.632	0.674	1.705	0.421	0.870	0.414
14	0.619	0.659	1.613	0.386	0.748	0.479
14.8	0.649	0.692	1.865	0.482	1.083	0.300
16.8	0.648	0.691	1.854	0.478	1.068	0.308
26.5	0.664	0.708	1.947	0.496	1.201	0.251

Table 2
Constituent volume fractions of bone tissues of children (HA = hydroxyapatite, col = collagen, H_2O = water).

Age (year)	ρ^{BM}	f_{HA} (-)	f_{col} (-)	f_{H2O} (-)
6	1.6	0.244	0.241	0.515
8	1.65	0.266	0.253	0.481
10	1.69	0.284	0.263	0.454
12	1.73	0.302	0.272	0.426
13	1.75	0.310	0.277	0.413

As far as the osteocyte mechanosensitivity is concerned, by comparing the two models the calculated difference were 11.7% (Figs. 8a–b) when μ was increased, and 10.1% (Figs. 8c–d) when it was decreased.

Effect of changes in bone tissue level composition on bone volume fraction

For the bone matrix stiffness tensors given in Table 3, the bone volume fraction evolution in a mm-sized trabecular bone sample was predicted and plotted in Fig. 9a by adopting the multiscale analytical model presented in the section entitled Analytical approach for bone remodeling simulations and the loading conditions and mechano-transduction parameters listed in Table 4. Each bone volume fraction evolution curve in Fig. 9a is characterized by a different volume fraction of collagen (nanometer scale) in the range of 0.243–0.277, and different volume fractions of water and hydroxyapatite see Table 2. Due to these differences in composition, a different elasticity tensor of the bone matrix (micrometer scale) results, and after remodeling, differences in bone volume fraction (millimeter scale) are found, ranging from 0.155 to 0.130 in the equilibrium state (Fig. 9b).

Discussion

In this study, a multiscale analytical model is proposed to simulate the bone adaptation at the tissue level while accounting for cell activity and material composition parameters at lower levels. The implementation of the multi-scale framework enabled us to describe the bone composition as a two-phase material at different levels. At the tissue level, it was modeled as a bone matrix with cylindrical voids. This assumption allowed for finding a closed-form solution for the mechanical stimulus sensed by the osteocytes. Such a mechanical stimulus was represented by a micromechanics-derived strain energy density based on an Eshelby matrix-inclusion problem that linked two different scales, typical RVE (mm) and pore (μm) scales, respectively, and accurately predicted the stress/strain states on the trabecular surface where it is hypothesized the bone remodeling is taking place. At the bone matrix level, the material was considered as a mineral foam of hydroxyapatite which is "reinforced" predominantly in the longitudinal direction by collagen fibrils as shown in [7,16]. This enabled us to describe the anisotropic elastic properties at higher levels as a function of this basic composition. Hence, the first goal of this study was accomplished even though the closed-form solution for the strain energy density was only possible when the inclusions dispersed in the matrix are assumed to have spherical or cylindrical geometry. The analytical results in terms of bone volume fraction evolution were compared to the corresponding numerical ones coming from a previously validated micro-FE-based bone remodeling algorithm [21,23]. In the investigated cases (see Figs. 5–8), the

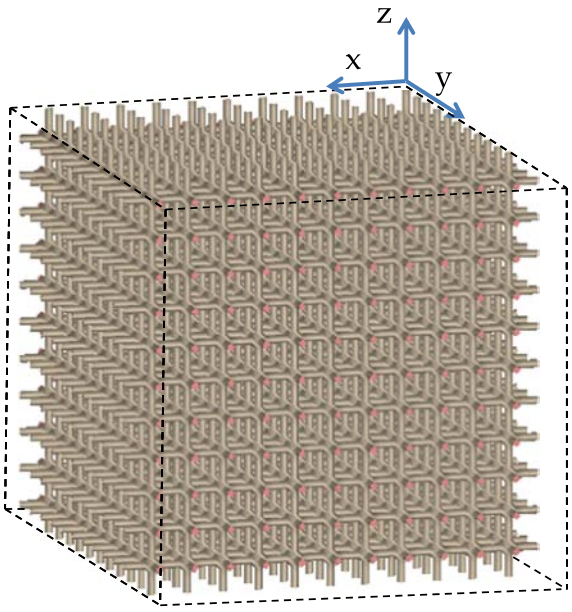

Fig. 4. Three-dimensional initial bone microstructure as a regular grid.

percentage difference between the results of the micro-FE model and the present multi-scale model at equilibrium was between 0.6 and 14.4%. Such agreement indicates that the micromechanics-derived strain energy density based on an Eshelby matrix-inclusion problem well represented the energy calculated in the micro-FE numerical while reducing the computational time by a factor of almost 1 million. The best agreement between analytical and numerical results is found with 0.6% difference at the equilibrium for the bone remodeling simulation (see Fig. 7) and 1% difference at the equilibrium when the bone formation time constant initial value is decreased by a factor of 10 (see Fig. 6). However, it should be noted that in the micro-FE model of bone remodeling trabecular bone material properties were assumed to be isotropic whereas in the multi-scale model they were anisotropic, with a higher stiffness in the trabecular longitudinal direction in which the collagen is oriented. The fact that good agreement in results was obtained is likely because the mechanical behavior at the bone tissue level is dominated by the modulus in the trabecular longitudinal direction: for the most common loading modes (compression, tension and bending), only the modulus in the longitudinal direction plays a role [43]. Hence, by specifying an isotropic modulus in the micro-FE models equal to the longitudinal modulus in the anisotropic multi-scale model, good agreement in mechanical behavior is expected. As a consequence, based on these observations it is further possible to implement easily the analytical model for whole bones applications (e.g. radius, femurs and vertebras) in which micro or continuum FE analysis and corresponding meshes under isotropic material assumption are exploited for the calculation of the micromechanics-based strain energy density.

Looking at the dynamic response of the analytical bone remodeling system, the model is found temporally stable and consistent with experimental observations of bone density changes during disuse and aging [44,45]. However, in the analytical simulations of Figs. 6c–d and Figs. 7c–d the BV/TV was not in agreement with the numerical results during

Table 3
Model-predicted stiffness tensor components of young healthy bone tissues.

Age (year)	C_{1111} (GPa)	C_{3333} (GPa)	C_{1122} (GPa)	C_{1133} (GPa)	C_{2323} (GPa)	C_{1212} (GPa)
6	10.514	13.390	4.855	5.402	2.946	2.826
8	11.708	14.811	5.142	5.754	3.415	3.283
10	12.779	16.098	5.401	6.065	3.837	3.690
12	13.696	17.548	5.692	6.407	4.307	4.138
13	14.613	18.343	5.853	6.592	4.562	4.380

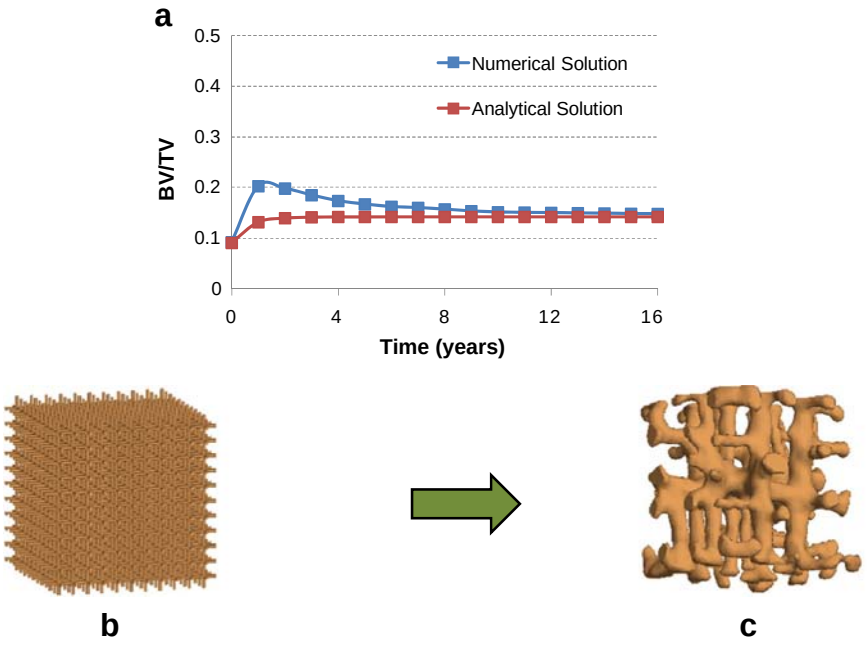

Fig. 5. Evolution of bone volume fraction (a) starting from a bone regular grid (b) and final adapted bone microstructure (c) during bone modeling.

the transient phase. This might relate to difference in the available free surface for both cell types between the analytical and numerical models. The response of the bone system in transient behavior can be further improved by changing parameters related to this free surface or by choosing optimal values for the time constant.

The third goal of this paper was to investigate the effects of collagen and hydroxyapatite changes at the nanometer scale on the bone volume fraction at the millimeter scale. Since the bone matrix of adult healthy tissue exhibits a stiffness which is time- and space-invariant when averaged over a millimeter-sized domain [26,29,30], and hence $\mathbb{C}_{BM}$ in Eq. (6) is constant for adult healthy tissue, it is interesting to also investigate diseased, medicated, or juvenile tissue, where this constancy is not observed. Since the elasticity of bone tissue in children changes with respect to age, the stiffness-dependent micro-mechanical signal sensed by the osteocytes is age-dependent as well, so that even age-independent osteocyte behavior cannot impede bone volume fractions from depending on age during development. This was demonstrated by the outcome of the micromechanical model and the multistep homogenization scheme adopted in this study which allowed taking into account the volume fraction of the elementary components (hydroxyapatite, collagen and water) of healthy children and to derive from this composition the elastic constants of the bone matrix. In turn, the elasticity tensors of the bone matrix determined different and associate strain energy density levels stored in the trabecular bone sample (millimeter level) and hence different predictions for the evolution of the bone volume fraction at the equilibrium state in the range of 0.13–0.15 (Fig. 9). These results suggest that the age-dependent nano-level properties in the bone matrix composition affect the cellular activities independently from the pre-existing architecture. The evolution of the bone volume fraction over the time is different in the range of age 6–13 years because of the increase in bone tissue mineralization during growth. The increased mineralization leads to an increase in bone tissue stiffness and thus lower strains in the bone tissue. As a consequence, the mechanical signal sensed by the osteocytes is reduced, which, in turn, affects the osteoblast activity. These results also suggest that younger healthy children have denser bones (i.e. lower vascular porosity) with respect to older healthy children. A reduction of bone density (i.e. an increase of vascular porosity) with age is also shown in [46] where the

Table 4
Parameter values used in the proposed multiscale analytical model.

Parameter	Symbol	Value	Unit
Bone formation time constant	τ	18	$\mu m^3/(nmol \cdot day)$
Osteocyte mechanosensitivity	μ	1.0	$nmol/(MPa \cdot \mu m^2)$
Bone resorption rate	A_{ocl}	0.17	$\mu m/day$
Applied stresses	σ_x	1.1	MPa
	σ_y	0.7	MPa
	σ_z	1.5	MPa
Bone specific surface fraction	α	0.8	-
Bulk modulus	k_{Fat}	1.33[a]	MPa
Bone matrix elastic constants	C_{1111}	$12.7 \cdot 103$[b]	MPa
	C_{1122}	$6.2 \cdot 10^3$[b]	MPa
	C_{1133}	$6.4 \cdot 10^3$[b]	MPa
	C_{3333}	$20.2 \cdot 10^3$[b]	MPa
Radial and circumferential Young's moduli	$E_1^* = E_2^*$	$9 \cdot 10^3$[b]	MPa
Axial Young's modulus	E_3^*	$18.8 \cdot 10^3$[b]	MPa

[a] [28].
[b] [31].

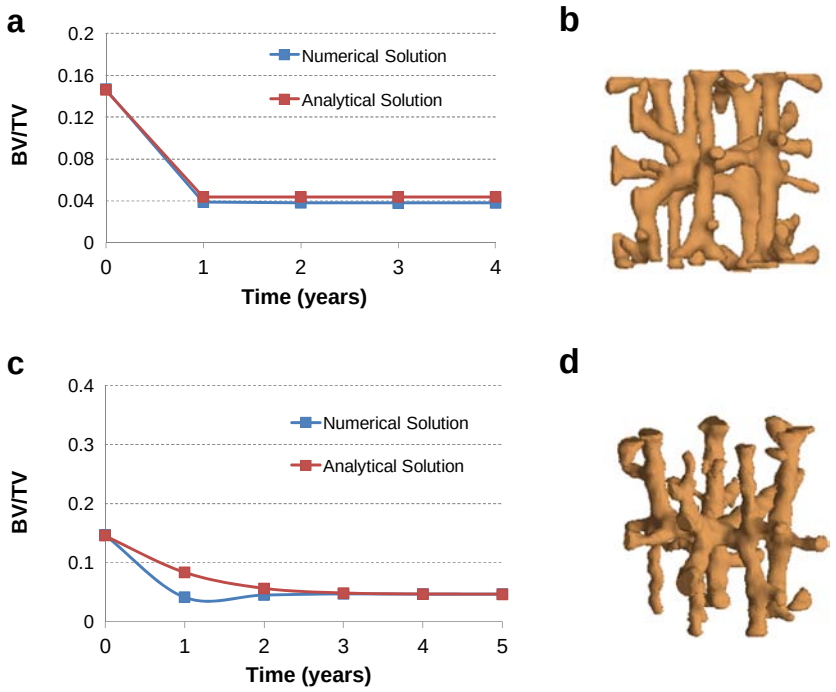

Fig. 6. Evolution of the bone volume fraction (a,c) and adaptation of the bone microstructure (b,d) when the initial osteoclast activity (A_{ocl}) is increased (a,b) and the initial osteoblast activity (τ) is decreased (c,d) by a factor of 10.

authors determined microstructural and strength variables of the distal radius of healthy girls by high-resolution peripheral computerized tomography and micro-finite element analysis and quantified low trabecular vBMD and thickness in the distal radius associated with reduced bone strength and increased fracture risk during growth. The aforementioned increase of vascular porosity is also consistent with the decrease of bone formation with increased age between 3 and 18 months, as evidenced by de Pollak et al. [47] in terms of histomorphometric indices.

A few limitations of the present study should be mentioned as well. First, at the tissue level the bone was modeled as a closed structure build of bone matrix with cylindrical voids whereas in reality it is an open structure and the voids shape is more complex. The reason for this simplification is that it enables finding analytical solutions. It would be possible to include more realistic microstructural models for the bone at this level. However, such models would require numerical approaches for the calculation of the SED and thus will require more

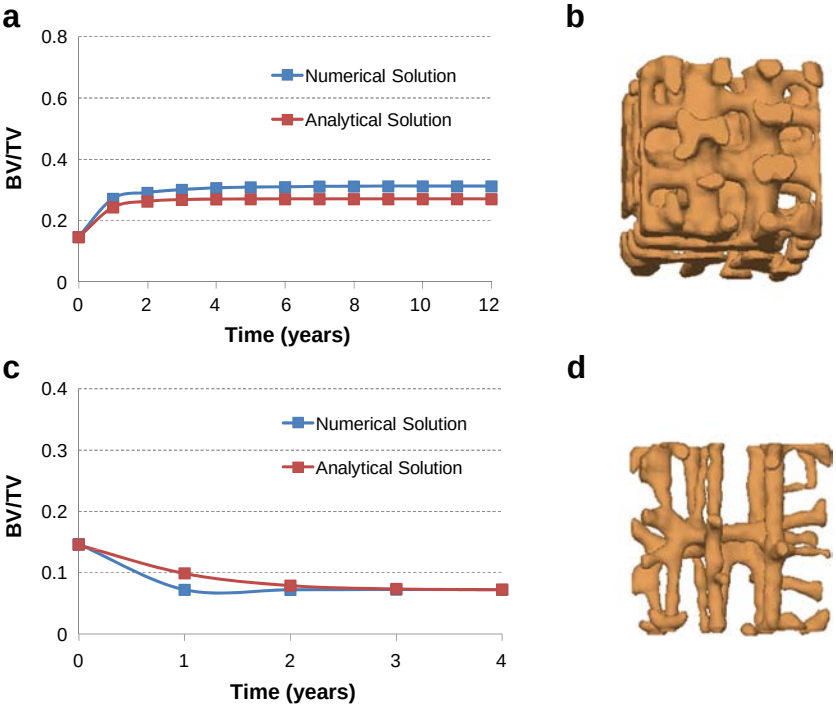

Fig. 7. Evolution of the bone volume fraction (a,c) and adaptation of the bone microstructure (b,d) when the loading magnitude ($\sigma_x, \sigma_y, \sigma_z$) is increased by 200% (a,b) and decreased by 50% (c,d).

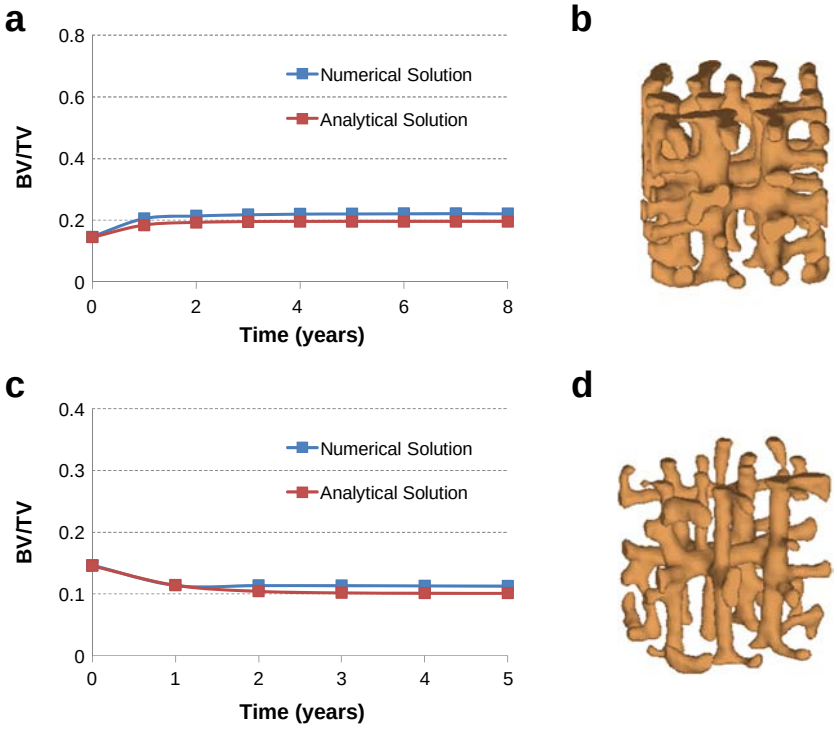

Fig. 8. Evolution of the bone volume fraction (a,c) and adaptation of the bone microstructure (b,d) when the osteocyte mechanosensitivity (μ) is increased by 200% (a,b) and decreased by 50% (c,d).

CPU time. Since the solutions of the numerical and analytical model based on the cylindrical voids model are very close, this model seems adequate. Second, in our study only the activity of the osteoblast cells was mechano-regulated, while the osteoclast activity was assumed to be not dependent on the mechanical stimulus. However, in the literature it is suggested that the osteocytes control both the osteoblast and osteoclast activities [48,49]. This choice was made to stay in agreement with the remodeling theory used in earlier numerical studies [15]. It should be noted, however, that it would be straightforward to also make osteoclast activity dependent on the mechanical signal, but in earlier studies this did not lead to large differences in the result [50]. Third, as in these earlier studies, we used strain energy density as the mechanical stimulus, whereas others have proposed other stimuli such as fluid flow and microdamage [11,51]. However, it was shown earlier that the results of the bone remodeling simulations are not very sensitive to the actual signal chosen [52]. Also, it should be mentioned that the framework developed here would enable analyses of fluid flow as well as microdamage, which take place at much lower levels than that of the bone structure. Fourth, we did not explicitly model the actual biochemical messenger pathways. Accounting for this in more detail as proposed by others [4,5] may further improve the simulations. Here also, we would like to emphasize that the framework developed in this investigation would enable accounting for such biochemical interactions. Still, we expect the main results of our study remain unaltered by introduction of the aforementioned further details. Fifth, the osteocyte microporosity was not included in the present formulation since it is assumed that the mechanical stimulus sensed by the osteocytes is the strain energy density in the extracellular matrix. The multi-step homogenization scheme based on micromechanics and adopted in this study, however, enables the inclusion of as many phases as required and could also represent the porosity of the lacunar–canalicular network. For example, lacunar porosity was considered in multiscale models for bone strength [53] as well as for fast and slow wave propagation and attenuation through the hierarchical lacunar–

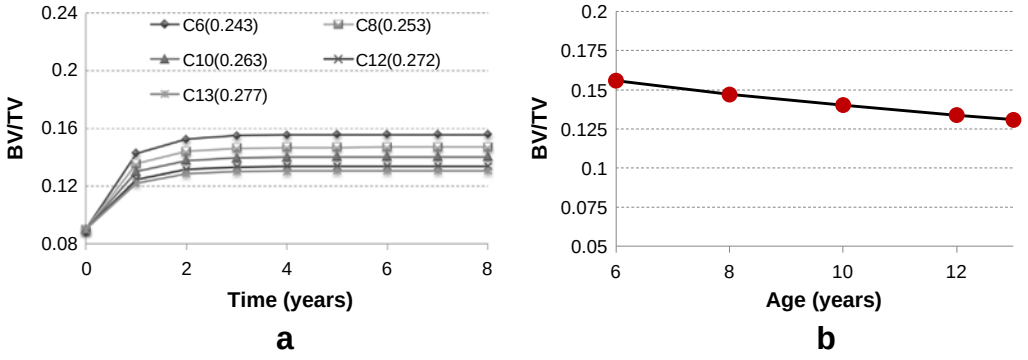

Fig. 9. (a) Evolution of the BV/TV at the millimeter scale as function of the volume fraction of collagen (f_{col}) at the nanometer scale during bone remodeling; (b) Predictions of bone volume fraction equilibrium values as function of the age of healthy children. In the plot legend, the nomenclature of each investigated case begins with the letter "C" (child), followed by the age of the child in year and the corresponding volume fraction of the collagen in brackets.

vascular pore system in bone [54]. Our present choice to take, as mechanical stimulus, the strain energy density in the extravascular bone matrix, is consistent with our approach to let the cells always deposit bone matrix of the same quality, i.e. with a constant osteocyte density (or lacunar porosity) per volume element of extravascular bone matrix. Interestingly, such a constant lacunar porosity across bone matrices of different ages or species actually suggests itself when one compares scanning electron micrographs from different anatomical sites [55,56]. Accordingly, when keeping the aforementioned idea of a constant "working mode" of the osteoblastic cells, then the additional explicit introduction of the lacunar–canalicular network would not alter any of our results. This is why we did not implement them for the scope and the contents of the present study. Coincidently, this choice has been also made in a recent multiscale systems biology-micromechanics approach [5]. However, extension of the model to the lacunar–canalicular network along the micromechanical lines sketched further above does make a lot of sense if one also wishes to test the effect of using alternative hypotheses for load adaptive bone remodeling at lower scales, e.g. fluid-flow and microdamage, on the density distribution at the organ level.

Finally, although our discussion was mainly focusing on the trabecular bone, the analytical approach can be straightforwardly applied to the cortical bone. Actually, the micromechanical representation depicted in Fig. 2 also holds for the latter, as was evidenced by various studies reporting satisfactory agreement between respective model predictions and corresponding experimental results [7,57,58].

Conclusions

The multiscale analytical model developed in this study for the simulation of bone remodeling relates the effects of structural changes at the nanometer level to changes in bone density at higher levels. Such an analytical formulation includes the feedback from the osteoclast/osteoblast activity and includes influences from mechanical stimuli and surface area available for remodeling. Furthermore, the multiscale analytical model allows for 1) coupling dynamic loading variables at the time scale of seconds to the adaptive processes at the scale of year; 2) for simultaneously exploring the effects of mechanobiological and geometric stimuli relating local loading conditions in the bone matrix to bone cells involved in bone remodeling; and 3) for taking into account of variations of collagen volume fraction that affects the stiffness of bone matrix linking the above mentioned scales (tissue and cell levels) to the third mineralized collagen level (100–500 nm). To the knowledge of the authors, it is the first time that in the literature such a novelty is found. The proposed model provides new insights on how mechanical properties and structures of bone at the organ level are affected by the mechanical properties and hierarchical structural levels at lower scales in both healthy and pathological conditions. Moreover, since our model's CPU demands are also dramatically, i.e. by the factor of 1 million, decreased as compared to conventional approaches in the field, it also holds the promise to provide an accurate and efficient tool for large scale patient-specific bone remodeling simulations in a clinical everyday setting, in particular for organs such as the hip or spine, where an accurate assessment of bone micro-architecture is not possible. In such analyses, the effect of macroscopic load transfer mechanisms, such as reduced trabecular load level due to the existence of thickening cortical shells, could be studied as well, in addition to the microscopic load transfer mechanism focused on in this paper.

Acknowledgments

The research leading to these results has received funding from the European Union Seventh Framework Programme (FP7/2007–2013) under grant agreement no 269909.

Appendix A

$\mathbb{A}_{BM}$ — *Strain concentration tensor*

$$A^{BM}_{1111} = [C_{1122}\,(C_{1122}-2k_{\mathrm{Fat}})(\phi-1) + C^2_{1111}\,(1+2\phi) + C_{1111}(2k_{\mathrm{Fat}}(1+\phi)-C_{1122}\phi)] / [(C_{1111}+C_{1122}+3C_{1111}\phi-C_{1122}\phi)(C_{1122}-2k_{\mathrm{Fat}})(\phi-1) + C_{1111}(1+\phi)] \quad (23)$$

$$A^{BM}_{1122} = [C_{1111}\,(C_{1111}-3C_{1122}+4k_{\mathrm{Fat}})\phi] / [(C_{1111}+C_{1122}+3C_{1111}\phi-C_{1122}\phi)(C_{1122}-2k_{\mathrm{Fat}})(\phi-1) + C_{1111}(1+\phi)] \quad (24)$$

$$A^{BM}_{1133} = [(k_{\mathrm{Fat}}-C_{1133})\phi] / [(C_{1122}-2k_{\mathrm{Fat}})(\phi-1) + C_{1111}(1+\phi)] \quad (25)$$

$$A^{BM}_{2211} = A^{BM}_{1122} \quad (26)$$

$$A^{BM}_{2222} = A^{BM}_{1111} \quad (27)$$

$$A^{BM}_{2233} = A^{BM}_{1133} \quad (28)$$

$$A^{BM}_{3311} = A^{BM}_{3322} = 0 \quad (29)$$

$$A^{BM}_{3333} = 1 \quad (30)$$

References

[1] Frost HM. Bone "mass" and the "mechanostat": A proposal. Anat Rec 1987;219(1):1–9.
[2] Cowin SC, Moss-Salentijn L, Moss ML. Candidates for the mechanosensory system in bone. J Biomech Eng 1991;113:191–7.
[3] Lemaire V, Tobin FL, Greller LD, Cho CR, Suva LJ. Modeling the interactions between osteoblast and osteoclast activities in bone remodeling. J Theor Biol 2004;229(3):293–309.
[4] Pivonka P, Zimak J, Smith DW, Gardiner BS, Dunstan CR, Sims NA, et al. Model structure and control of bone remodeling: a theoretical study. Bone 2008;43(2):249–63.
[5] Scheiner S, Pivonka P, Hellmich C. Coupling systems biology with multiscale mechanics, for computer simulations of bone remodeling. Comput Methods Appl Mech Eng 2013;254:181–96.
[6] Rho JY, Kuhn-Spearing L, Zioupos P. Mechanical properties and the hierarchical structure of bone. Med Eng Phys 1998;20(2):92–102.
[7] Hellmich C, Ulm FJ, Dormieux L. Can the diverse elastic properties of trabecular and cortical bone be attributed to only a few tissue-independent phase properties and their interactions? Biomech Model Mechanobiol 2004;2:219–38.
[8] Currey JD. The structure and mechanics of bone. J Mater Sci 2012;47:41–54.
[9] Parfitt AM. Osteonal and hemi-osteonal remodeling: the spatial and temporal framework for signal traffic in adult human bone. J Cell Biochem 1994;55(3):273–86.
[10] Eriksen EF, Kassem M. The cellular basis of bone remodeling. Triangle 1992;31:45–57.
[11] Andreaus U, Colloca M, Iacoviello D. An optimal control procedure for bone adaptation under mechanical stimulus. Control Eng Pract 2012;20(6):575–83.
[12] Kameo Y, Adachi T, Hojo M. Effects of loading frequency on the functional adaptation of trabeculae predicted by bone remodeling simulation. J Mech Behav Biomed Mater 2011;4(6):900–8.
[13] Webster D, Müller R. In silico models of bone remodeling from macro to nano—from organ to cell. Wiley Interdiscip Rev Syst Biol Med 2011;3(2):241–51.
[14] Ruimerman R, Hilbers P, van Rietbergen B, Huiskes R. A theoretical framework for strain-related trabecular bone maintenance and adaptation. J Biomech 2005;38(4):931–41.
[15] Huiskes R, Ruimerman R, Van Lenthe GH, Janssen JD. Effects of mechanical forces on maintenance and adaptation of form in trabecular bone. Nature 2000;405(6787):704–6.
[16] Fritsch A, Hellmich C. Universal microstructural patterns in cortical and trabecular, extracellular and extravascular bone materials: Micromechanics-based prediction of anisotropic elasticity. J Theor Biol 2007;244(4):597–620.

[17] Coelho PG, Rui Fernandes P, Carriço Rodrigues H. Multiscale modeling of bone tissue with surface and permeability control. J Biomech 2011;44(2):321–9.
[18] Hambli R, Katerchi H, Benhamou CL. Multiscale methodology for bone remodelling simulation using coupled finite element and neural network computation. Biomech Model Mechanobiol 2011;10(1):133–45.
[19] Podshivalov L, Fischer A, Bar-Yoseph PZ. 3D hierarchical geometric modeling and multiscale FE analysis as a base for individualized medical diagnosis of bone structure. Bone 2011;48(4):693–703.
[20] Colloca M, van Rietbergen B, Blanchard R, Hellmich C, Ito K. From cell level to organ level: a multiscale approach for bone remodeling simulation. J Biomech 2012;45: S470.
[21] Colloca M, Ito K, van Rietbergen B. An analytical approach to investigate the evolution of bone volume fraction in bone remodeling simulation at the tissue and cell level. J Biomech Eng 2014;136(3):031004. http://dx.doi.org/10.1115/1.4026227.
[22] Fazzalari NL, Kuliwaba JS, Forwood MR. Cancellous bone microdamage in the proximal femur: influence of age and osteoarthritis on damage morphology and regional distribution. Bone 2002;31(6):697–702.
[23] Colloca M, Blanchard R, Hellmich C, Ito K, van Rietbergen B. Evolution of bone volume fraction in bone remodeling: a multiscale analytical investigation. Proceedings of the 11th International Symposium on Computer Methods in Biomechanics and Biomedical Engineering. Taylor & Francis Group; 2013.
[24] Martin RB. Porosity and specific surface of bone. Crit Rev Biomed Eng 1984; 10(3):179.
[25] Zaoui A. Continuum micromechanics: survey. J Eng Mech ASCE 2002;128(8): 808–16.
[26] Hellmich C, Kober C, Erdmann B. Micromechanics-based conversion of CT data into anisotropic elasticity tensors, applied to Fe simulations of a mandible. Ann Biomed Eng 2008;36(1):108–22.
[27] Hellmich C, Barthélémy J-F, Dormieux L. Mineral–collagen interactions in elasticity of bone ultrastructure—a continuum micromechanics approach. Eur J Mech A Solid 2004;23(5):783–810.
[28] Linder-Ganz E, Amit G. Mechanical compression-induced pressure sores in rat hindlimb: muscle stiffness, histology, and computational models. J Appl Physiol 2004;96(6):2034–49.
[29] Hoffler CE, Moore KE, Kozloff K, Zysset PK, Goldstein SA. Age, gender, and bone lamellae elastic moduli. J Orthop Res 2000;18:432–7.
[30] Feng L, Jasiuk I. Multi-scale characterization of swine femoral cortical bone. J Biomech 2011;44(2):313–20.
[31] Malandrino A, Fritsch A, Lahayne O, Kropik K, Redl H, Noailly JRM, et al. Anisotropic tissue elasticity in human lumbar vertebra, by means of a coupled ultrasound-micromechanics approach. Mater Lett 2012;78:154–8.
[32] Currey J. Changes in the impact energy absorption of bone with age. J Biomech 1979;12:459–69.
[33] Vuong J, Hellmich C. Bone fibrillogenesis and mineralisation: quantitative analysis and implications for tissue elasticity. J Theor Biol 2011;287:115–30.
[34] Gong J, Arnold J, Cohn SH. The density of organic and volatile and non-volatile inorganic components of the bone. Anat Rec 1964;149:319–24.
[35] Lees S. Considerations regarding the structure of the mammalian mineralized osteoid from viewpoint of the generalized packing model. Connect Tissue Res 1987;16(4):281–303.
[36] Gong JK, Arnold JS, Cohn SH. Composition of trabecular and cortical bone. Anat Rec 1964;149(3):325–32.
[37] Hellmich C. Microelasticity of bone. In: Dormieux L, Ulm F-J, editors. Applied Micromechanics of Porous Media, CISM, vol. 480. Wien-New York: Springer; 2005. p. 289–332.
[38] Jaworski M, Lebiedowski M, Lorenc RS, Trempe J. Ultrasound bone measurement in pediatric subjects. Calcif Tissue Int 1995;56(5):368–71.
[39] van Rietbergen B, Weinans HH, Huiskes R, Polman BJW. Computational strategies for iterative solutions of large FEM applications employing voxel data. Int J Numer Methods Eng 1996:2743–67.
[40] Christen P, Ito K, Mueller R, Rubin MR, Dempster DW, Bilezikian JP, et al. Patient-specific bone modelling and remodelling simulation of hypoparathyroidism based on human iliac crest biopsies. J Biomech 2012;45:2411–6.
[41] Garnero P, Sornay-Rendu E, Chapuy MC, Delmas PD. Increased bone turnover in late postmenopausal women is a major determinant of osteoporosis. J Bone Miner Res 1996;11(3):337–49.
[42] Eckstein F, Burstein D, Link TM. Quantitative MRI of cartilage and bone: degenerative changes in osteoarthritis. NMR Biomed 2006;19:822–54.
[43] Verhulp E, van Rietbergen B, Huiskes R. Comparison of micro-level and continuum-level voxel models of the proximal femur. J Biomech 2006;39(16):2951–7.
[44] Li XJ, Jee WSS, Chow SY, Woodbury DM. Adaptation of cancellous bone to aging and immobilization in the rat: a single photon absorptiometry and histomorphometry study. Anat Rec 1990;227(1):12–24.
[45] Fyhrie DP, Schaffler MB. The adaptation of bone apparent density to applied load. J Biomech 1995;28(2):135–46.
[46] Chevalley T, Bonjour J, van Rietbergen B, Rizzoli R, Ferrari S. Fractures in healthy females followed from childhood to early adulthood are associated with later menarcheal age and with impaired bone microstructure at peak bone mass. J Clin Endocrinol Metab 2012;97:4174–81.
[47] De Pollak C, Arnaud E, Renier D, Marie PJ. Age-related changes in bone formation, osteoblastic cell proliferation, and differentiation during postnatal osteogenesis in human calvaria. J Cell Biomech 1997;64(1):128–39.
[48] Sommerfeldt D, Rubin C. Biology of bone and how it orchestrates the form and function of the skeleton. Eur Spine J 2001;10(2):S86–95.
[49] Lau E, Al-Dujaili S, Guenther A, Liu D, Wang L, You L. Effect of low-magnitude, high-frequency vibration on osteocytes in the regulation of osteoclasts. Bone 2010;46(6): 1508–15.
[50] van Oers RF, Ruimerman R, Tanck E, Hilbers PA, Huiskes R. A unified theory for osteonal and hemi-osteonal remodeling. Bone 2008;42(2):250–9.
[51] Burger EH, Klein-Nulend J. Mechanotransduction in bone-role of the lacuno–canalicular network. FASEB J 1999;13:S101–12.
[52] Ruimerman R, van Rietbergen B, Hilbers P, Huiskes R. The effects of trabecular-bone loading variables on the surface signaling potential for bone remodeling and adaptation. Ann Biomed Eng 2005;33(1):71–8.
[53] Fritsch A, Hellmich Ch, Dormieux L. Ductile sliding between mineral crystals followed by rupture of collagen crosslinks: experimentally supported micromechanical explanation of bone strength. J Theor Biol 2009;260:230–52.
[54] Morin C, Ch Hellmich. A multiscale poromicromechanical approach to wave propagation and attenuation in bone. Ultrasonics 2014;54:1251–69.
[55] Tai K, Pelled G, Sheyn D, Bershteyn A, Han L, Kallai I, et al. Nanobiomechanics of repair bone regenerated by genetically modified mesenchymal stem cells. Tissue Eng A 2008;14:1709–20.
[56] Buckwalter J, Glimcher M, Cooper R, Recker R. Bone biology, part I: structure, blood supply, cells, matrix, and mineralization. J Bone Joint Surg 1995;77A:1256–75.
[57] Granke M, Grimal Q, Saied A, Nauleau P, Peyrin F, Laugier P. Change in porosity is the major determinant of the variation of cortical bone elasticity at the millimeter scale in aged women. Bone 2011;49:1020–6.
[58] Hamed E, Lee Y, Jasiuk I. Multiscale modeling of elastic properties of cortical bone. Acta Mech 2010;213:131–54.